

Constraint-damping of the CCZ4 formulation in simulations of binary neutron stars

Daniela Alic,¹ Wolfgang Kastaun,¹ and Luciano Rezzolla^{1,2}

¹Max-Planck-Institut für Gravitationsphysik, Albert-Einstein-Institut, Potsdam, 14476, Germany

²Institute for Theoretical Physics, Max-von-Laue-Str. 1, 60438 Frankfurt am Main, Germany

Following previous work in vacuum spacetimes, we investigate the constraint-damping properties in the presence of matter of the recently developed conformal, traceless, and covariant CCZ4 formulation of the Einstein equations. First, we evolve an isolated neutron star with an ideal gas equation of state and subject to a constraint-violating perturbation. We compare the evolution of the constraints using the CCZ4 and BSSNOK systems. Second, we study the collapse of an unstable spherical star to a black hole. Finally, we evolve binary neutron star systems over several orbits until the merger, the formation of a black hole, and up to the ringdown. We show that the CCZ4 formulation is stable in the presence of matter and that the constraint violations are one or more orders of magnitude smaller than for the BSSNOK formulation. Furthermore, by comparing the CCZ4 and the BSSNOK formulations also for neutron star binaries with large initial constraint violations, we investigate their influence on the errors on physical quantities. We also give a new, simple and robust prescription for the damping parameter that removes the instabilities found when using the fully covariant version of CCZ4 in the evolution of black holes. Overall, we find that at essentially the same computational costs the CCZ4 formulation provides solutions that are stable and with a considerably smaller violation of the Hamiltonian constraint than the BSSNOK formulation. We also find that the performance of the CCZ4 formulation is very similar to another conformal and traceless, but non-covariant formulation of the Z4 system, *i.e.*, the Z4c formulation.

PACS numbers: 04.25.dk, 04.25.Nx, 04.30.Db, 04.40.Dg, 95.30.Sf, 97.60.Jd

I. INTRODUCTION

Recent developments in numerical relativity allow for the simulation of binary compact objects, *e.g.*, binary neutron star (NS) systems, which are among the strongest sources of gravitational waves. Given that less than one decade ago, even the vacuum binary black-hole (BH) problem was still a challenge for numerical evolutions of the Einstein equations, the progress is indeed remarkable. Part of this rapid progress is surely due to a better understanding of the mathematical properties of the different formulations of the Einstein equations and of the choice of suitable gauge conditions. The most widely used formulation of the Einstein equations in three-dimensional (3D) numerical simulations is given by a conformal and traceless formulation of the ADM (Arnowitt-Deser-Misner) 3+1 decomposition of the Einstein equations [1, 2], and is also known as the BSSNOK (or BSSN) formulation [3–5].

Another conformal and traceless formulation, *i.e.*, the conformal and covariant CCZ4 formulation, was introduced recently in Ref. [6] (hereafter paper I), where we discussed in detail its structure and properties. The CCZ4 formulation shares some important properties with BSSNOK. It allows for stable evolutions in conjunction with robust and singularity-avoiding gauges, thus eliminating the need for excision techniques, and with simple Sommerfeld radiative boundary conditions. The main advantage of the CCZ4 formulation over the BSSNOK formulation is its ability to dynamically evolve the constraints equations and to couple them with a constraint-damping scheme that leads to a rapid suppression of the violations that are inevitably produced in numerical simulations.

In paper I we validated the properties of the CCZ4 system in evolutions of single and binary BH systems. The constraint propagating and damping properties of the system turned out to be very useful in reducing the violations produced in long-

term simulations and lead to constraint violations that were, on average, one order of magnitude smaller than those with the BSSNOK system. In this work, we investigate the behavior of the CCZ4 system also in evolutions of non-vacuum spacetimes, in particular of single and binary NSs. In paper I, the simulations were performed with both a multi-patch coordinate system, where the spherical outer boundary was causally disconnected, and Cartesian grids plus radiative boundary conditions. In the latter, we noticed reflections from the outer boundary which led to an increase in the values of the constraints. However, these violations were rapidly damped and there was no sign of instabilities produced in relation with the outer boundary. In this work, we focus on the latter case which is used more often in simulations of neutron star mergers.

We recall that the CCZ4 system contains three constant parameters, one of which (κ_3 , see below) determines if the system is actually covariant or not (throughout this paper we refer to both versions as CCZ4). While both cases were studied in paper I, we also found there that exponentially growing modes appear for the fully covariant system. An important point of this paper is the exploration of the behavior of both versions of the CCZ4 system in spacetimes containing matter. We will show that the aforementioned instabilities occur only when a BH is present in the spacetime, while simulations of NSs do not show such instabilities. Furthermore, we will also demonstrate that even when a BH appears in the solution, *e.g.*, in the collapse of a NS, or after the merger of two NSs, a modification of the damping terms results in stable evolutions of the fully covariant CCZ4 system. Finally, we will also confirm that in all comparisons between the covariant and the non-covariant versions of the CCZ4 system the differences between the results are very small.

A different conformal version of the non-covariant Z4 system has been presented in Ref. [7–11]. This system, called

Z4c, removes source terms in order to bring the evolution equations in a form which is closer to BSSNOK system. Recent numerical results obtained with Z4c in 3D simulations of compact objects [11] report a reduction in the Hamiltonian constraint violation between one and three orders of magnitude in respect to BSSNOK for non-vacuum spacetimes, and between one and two orders of magnitude for black hole spacetimes. Performing a similar comparison of the Z4c and BSSNOK systems, we could not confirm all their results, probably because the important improvement associated with Z4c comes from the use of constraint preserving boundary conditions, of the type described in Ref. [8]. The direct comparison between the CCZ4 and Z4c systems shows that the CCZ4 leads to similarly low constraint violations and allows long term stable evolution when coupled with standard radiative boundary conditions. There are no features intrinsic to the Z4c which suggest improvement over CCZ4.

The plan of the paper is as follows. Section II presents an overview of the CCZ4 system of the Einstein equations coupled with the hydrodynamic equations, as well as the numerical infrastructure of our simulations. Section III is dedicated to numerical results obtained with the CCZ4 system in evolutions of a stable isolated NS, the collapse of an unstable NS to a BH and of binary NS systems, both with constraint-satisfying and constraint-violating initial data. In the first four subsections, we compare results obtained with the BSSN and CCZ4 formulations of the Einstein equations, while the last two subsections are dedicated to a comparison with the Z4c system and between the fully covariant and the non-covariant versions of the CCZ4. We conclude with the summary and

discussions in Section IV.

Throughout this paper we use a metric signature of $(-, +, +, +)$ and units in which $c = G = M_\odot = 1$, unless noted otherwise. Greek indices are taken to run from 0 to 3, Latin indices from 1 to 3 and we adopt the standard convention for the summation over repeated indices.

II. FORMULATION AND NUMERICAL METHODS

A. The CCZ4 system

The CCZ4 system is a conformal and covariant formulation of the Einstein equations. It is based on a conformal transformation of the Z4 system (see paper I), which converts the original Hamiltonian and momentum ADM constraints into evolution equations for a four-vector Z_μ . This amounts to introducing two additional evolution variables, namely the projection Θ along the normal direction of the four-vector Z_μ and its spatial component Z_i . The system can be supplemented with damping terms [12], which ensure exponential damping of the constraint violations in numerical evolutions.

The steps required to convert the original Z4 system in a conformal version were presented in our previous paper I. For completeness, we summarize here the main ideas behind the Z4 formulation and point to [13, 14] for more details about its properties. The CCZ4 system is given by the following set of evolution equations:

$$\partial_t \tilde{\gamma}_{ij} = -2\alpha \tilde{A}_{ij}^{\text{TF}} + 2\tilde{\gamma}_{k(i} \partial_{j)} \beta^k - \frac{2}{3} \tilde{\gamma}_{ij} \partial_k \beta^k + \beta^k \partial_k \tilde{\gamma}_{ij}, \quad (1)$$

$$\begin{aligned} \partial_t \tilde{A}_{ij} &= \phi^2 [-\nabla_i \nabla_j \alpha + \alpha (R_{ij} + \nabla_i Z_j + \nabla_j Z_i - 8\pi S_{ij})]^{\text{TF}} + \alpha \tilde{A}_{ij} (K - 2\Theta) \\ &\quad - 2\alpha \tilde{A}_{il} \tilde{A}_j^l + 2\tilde{A}_{k(i} \partial_{j)} \beta^k - \frac{2}{3} \tilde{A}_{ij} \partial_k \beta^k + \beta^k \partial_k \tilde{A}_{ij}, \end{aligned} \quad (2)$$

$$\partial_t \phi = \frac{1}{3} \alpha \phi K - \frac{1}{3} \phi \partial_k \beta^k + \beta^k \partial_k \phi, \quad (3)$$

$$\partial_t K = -\nabla^i \nabla_i \alpha + \alpha (R + 2\nabla_i Z^i + K^2 - 2\Theta K) + \beta^j \partial_j K - 3\alpha \kappa_1 (1 + \kappa_2) \Theta + 4\pi \alpha (S - 3\tau), \quad (4)$$

$$\partial_t \Theta = \frac{1}{2} \alpha \left(R + 2\nabla_i Z^i - \tilde{A}_{ij} \tilde{A}^{ij} + \frac{2}{3} K^2 \right) \boxed{-2\Theta K} \boxed{-Z^i \partial_i \alpha} + \beta^k \partial_k \Theta - \alpha \kappa_1 (2 + \kappa_2) \Theta - 8\pi \alpha \tau, \quad (5)$$

$$\begin{aligned} \partial_t \hat{\Gamma}^i &= 2\alpha \left(\tilde{\Gamma}_{jk}^i \tilde{A}^{jk} - 3\tilde{A}^{ij} \frac{\partial_j \phi}{\phi} - \frac{2}{3} \tilde{\gamma}^{ij} \partial_j K \right) + 2\tilde{\gamma}^{ki} \left(\alpha \partial_k \Theta \boxed{-\Theta \partial_k \alpha - \frac{2}{3} \alpha K Z_k} \right) - 2\tilde{A}^{ij} \partial_j \alpha \\ &\quad + \tilde{\gamma}^{kl} \partial_k \partial_l \beta^i + \frac{1}{3} \tilde{\gamma}^{ik} \partial_k \partial_l \beta^l + \frac{2}{3} \tilde{\Gamma}^i \partial_k \beta^k - \tilde{\Gamma}^k \partial_k \beta^i \boxed{+2\kappa_3 \left(\frac{2}{3} \tilde{\gamma}^{ij} Z_j \partial_k \beta^k - \tilde{\gamma}^{jk} Z_j \partial_k \beta^i \right)} \\ &\quad + \beta^k \partial_k \hat{\Gamma}^i - 2\alpha \kappa_1 \tilde{\gamma}^{ij} Z_j - 16\pi \alpha \tilde{\gamma}^{ij} S_j, \end{aligned} \quad (6)$$

where $\tilde{\gamma}_{ij} = \phi^2 \gamma_{ij}$ is the conformal metric with unit determinant $\phi = (\det(\gamma_{ij}))^{-1/6}$, while the extrinsic curvature K_{ij} is represented by its trace $K \equiv K_{ij} \gamma^{ij}$ and its trace-free com-

ponents

$$\tilde{A}_{ij} = \phi^2 (K_{ij} - \frac{1}{3} K \gamma_{ij}). \quad (7)$$

The three-dimensional Ricci tensor R_{ij} is split into a part \tilde{R}_{ij}^ϕ containing conformal terms and another one, \tilde{R}_{ij} , con-

taining space derivatives of the conformal metric, defined as

$$\tilde{R}_{ij} = -\frac{1}{2}\tilde{\gamma}^{lm}\partial_l\partial_m\tilde{\gamma}_{ij} + \tilde{\gamma}_{k(i}\partial_{j)}\tilde{\Gamma}^k + \tilde{\Gamma}^k\tilde{\Gamma}_{(ij)k} + \tilde{\gamma}^{lm}\left[2\tilde{\Gamma}_{l(i}\tilde{\Gamma}_{j)km} + \tilde{\Gamma}_{im}^k\tilde{\Gamma}_{kj}l\right], \quad (8)$$

$$\tilde{R}_{ij}^\phi = \frac{1}{\phi^2}\left[\phi\left(\tilde{\nabla}_i\tilde{\nabla}_j\phi + \tilde{\gamma}_{ij}\tilde{\nabla}^l\tilde{\nabla}_l\phi\right) - 2\tilde{\gamma}_{ij}\tilde{\nabla}^l\phi\tilde{\nabla}_l\phi\right]. \quad (9)$$

The following definitions apply for matter-related quantities

$$\tau \equiv n_\mu n_\nu T^{\mu\nu}, \quad S_i \equiv n_\nu T^\nu_i, \quad S_{ij} \equiv T_{ij}, \quad (10)$$

and Θ is the projection of the Z4 four-vector along the normal direction, $\Theta \equiv n_\mu Z^\mu = \alpha Z^0$. We note that we here follow the definition of the normal four-vector suggested in Ref. [13], *i.e.*, $n_\mu = (\alpha, 0)$ and $n^\mu = (-1/\alpha, \beta^i/\alpha)$, which is different from the more traditional one in which $n_\mu = (-\alpha, 0)$ and $n^\mu = (1/\alpha, -\beta^i/\alpha)$. These different definitions do not affect the form of the CCZ4 equations.

The evolution variable Z_i of the Z4 formulation is now included in the $\tilde{\Gamma}^i$ variable of the CCZ4 formulation

$$\hat{\Gamma}^i \equiv \tilde{\Gamma}^i + 2\tilde{\gamma}^{ij}Z_j, \quad (11)$$

where

$$\tilde{\Gamma}^i \equiv \tilde{\gamma}^{jk}\tilde{\Gamma}_{jk}^i = \tilde{\gamma}^{ij}\tilde{\gamma}^{kl}\partial_l\tilde{\gamma}_{jk}. \quad (12)$$

The numerical simulations presented in this paper use as gauge conditions the “1 + log” slicing

$$\partial_t\alpha = -2\alpha(K - 2\Theta) + \beta^k\partial_k\alpha, \quad (13)$$

and the Gamma-driver shift condition

$$\partial_t\beta^i = fB^i + \beta^k\partial_k\beta^i, \quad (14)$$

$$\partial_tB^i = \partial_t\hat{\Gamma}^i - \beta^k\partial_k\hat{\Gamma}^i + \beta^k\partial_kB^i - \eta B^i, \quad (15)$$

where the gauge parameter f is set to 3/4. We adopt the “*constrained approach*” from paper I in order to enforce the constraints of the conformal formulation (trace cleaning).

We also compute the constraint violations introduced by the numerical evolution in the ADM constraints

$$H = R - K_{ij}K^{ij} + K^2 - 16\pi\tau, \quad (16)$$

$$M_i = \gamma^{jl}(\partial_lK_{ij} - \partial_iK_{jl} - \Gamma_{jl}^mK_{mi} + \Gamma_{ji}^mK_{ml}) - 8\pi S_i. \quad (17)$$

For both the BSSNOK and the CCZ4 systems, we compute the ADM quantities from the evolved variables of the two systems.

We recall that the parameters κ_1 and κ_2 control the damping terms and that all the constraint-related modes are damped

when $\kappa_1 > 0$ and $\kappa_2 > -1$ [12]. The third coefficient κ_3 , instead, affects some quadratic terms in the evolution Eq. (6) for $\hat{\Gamma}^i$ and determines the covariance of the corresponding CCZ4 system. In particular, a value of $\kappa_3 = 1$ corresponds to full covariance.

We also recall that in paper I we performed numerical experiments with the covariance parameter κ_3 and concluded that a choice of $\kappa_3 = 1$ and $\kappa_1 = \text{const.}$ leads to unstable behavior in the context of black-hole spacetimes. Even though we could not fully isolate the cause of these numerical instabilities, we found that they are produced by nonlinear couplings with the damping terms, which are important for reducing the violations in the constraints. As a result, all of the tests reported in paper I made use of $\kappa_3 = 1/2$, which, for consistency with paper I, is also the value we will use for the majority of the tests discussed here. Two important remarks should however be made now, although they will be discussed also later on. First, in the presence of a non-singular spacetime with matter, a fully covariant formulation (*i.e.*, with $\kappa_3 = 1$) does not show any of the pathologies encountered in paper I with black holes. The pathologies however do appear as soon as a black hole is formed. Second, we have devised a new prescription for the damping term κ_1 which couples it to the lapse function and cures these instabilities also when black holes appear in the evolution. As a result, independently of whether we are considering vacuum or non-vacuum spacetimes, our CCZ4 formulation can now *always* be used in its fully covariant form. A more extended discussion of this point, with the presentation a series of examples, is postponed to Section III F.

As mentioned in the Introduction, another non-covariant but conformal formulation of the Z4 system has been proposed recently in Ref. [11], namely, the Z4c formulation. The suggestion behind the Z4c formulation is that of introducing the damping features of the Z4 formulation with only minimal changes to the BSSNOK system. As we will comment later on, this strategy is very reasonable one and leads to results that are comparable to those of the CCZ4 formulation and whose main drawback is that of being non-covariant. While this aspect of the formulation may be harmless in practice, it makes it difficult to generalize the properties found in a particular coordinate system, leaving room for unexpected behavior.

Because the CCZ4 and the Z4c formulations differ only in non-principal part terms, we have marked the terms that are

missing in the Z4c formulation with blue boxes within the set of evolution equations (1)–(6). In addition, the Z4c system evolves the trace of the extrinsic curvature \hat{K} using an evolution equation similar to the BSSNOK one [11]

$$\begin{aligned} \partial_t \hat{K} = & -\nabla^i \nabla_i \alpha + \alpha \left(\tilde{A}_{ij} \tilde{A}^{ij} + \frac{1}{3} (\hat{K} + 2\Theta)^2 \right) \\ & + \beta^j \partial_j \hat{K} + \alpha \kappa_1 (1 - \kappa_2) \Theta + 4\pi \alpha (S + \tau), \end{aligned} \quad (18)$$

to replace Eq. (4). This variable can be translated in CCZ4 terms as

$$\hat{K} = K^{\text{BSSNOK}} = K - 2\Theta. \quad (19)$$

B. The relativistic hydrodynamic equations

We evolve the hydrodynamic equations in flux-conservative form as

$$\partial_t \hat{D} = -\partial_k \left[w^k \hat{D} \right], \quad (20)$$

$$\begin{aligned} \partial_t \hat{\tau} = & -\partial_k \left[w^k \hat{\tau} + \phi^{-3} \alpha p v^k \right] \\ & + \alpha \hat{S}^{lm} K_{lm} - \hat{S}^k \partial_k \alpha, \end{aligned} \quad (21)$$

$$\begin{aligned} \partial_t \hat{S}_i = & -\partial_k \left[w^k \hat{S}_i + \phi^{-3} \alpha p \delta_i^k \right] \\ & + \frac{\alpha}{2} \hat{S}^{lm} \partial_i \gamma_{lm} + \hat{S}_k \partial_i \beta^k - (\hat{\tau} + \hat{D}) \partial_i \alpha. \end{aligned} \quad (22)$$

The evolved variables are the conserved density \hat{D} , the conserved energy density $\hat{\tau}$, and the conserved momentum density \hat{S}_i , whose definition is given by

$$\hat{D} \equiv \phi^{-3} \rho W, \quad (23)$$

$$\hat{\tau} \equiv \phi^{-3} (\rho h W^2 - p) - \hat{D}, \quad (24)$$

$$\hat{S}_i \equiv \phi^{-3} \rho h W^2 v_i. \quad (25)$$

Above, ρ is the rest mass density, v^i is the 3-velocity, W is the Lorentz factor, $w^i \equiv \alpha v^i - \beta^i$ is the advection speed with respect to the coordinates, p is the pressure, ϵ is the specific internal energy, and $h = 1 + \epsilon + p/\rho$ is the specific enthalpy. Finally, the projection of the energy-momentum tensor onto the spatial hypersurfaces of the foliation leads to the spatial tensor

$$\hat{S}_{ij} \equiv \phi^{-3} (\rho h W^2 v_i v_j + \gamma_{ij} p). \quad (26)$$

C. Numerical Setup

To evolve the hydrodynamic equations, we rely on an improved version of the `Whisky` code described in [15–19], but without making use of the ideal-MHD part or of the high-order finite-difference operators. The evolution of the spacetime is performed using our CCZ4 implementation within the `McLachlan` code [20], which is part of the publicly available

Einstein Toolkit infrastructure based on the `Cactus` computational framework. For the time integration we are using the method of lines with an explicit 4th-order Runge-Kutta method. We employ adaptive mesh refinement (AMR) for our numerical grid, provided via the `Carpet` driver [21]. For single star simulations, we use a fixed grid hierarchy, while for binary NS runs we follow the centers-of-mass of the stars with moving refined boxes. During the merger, those are replaced by larger non-moving refinement regions of the same resolution. Shortly after, one more refinement level with doubled resolution is activated to better resolve the black hole.

For the solution of the Einstein equations we use finite-difference spatial differential operators of various orders, although the results presented in this paper have been obtained using 4th-order accurate schemes. The spatial discretization of the hydrodynamic equations, on the other hand, uses a finite-volume high-resolution shock-capturing scheme adopting the parabolic reconstruction of the piecewise parabolic method (PPM) [22], and the Harten-Lax-van Leer-Einfeldt (HLL) [23] approximate Riemann solver. In contrast to the original `Whisky` code, we do not reconstruct the 3-velocities v^i , but the quantities $W v^i$ (as done in Ref. [18]). This guarantees that the velocities reconstructed at the cell boundaries stay subluminal even under the extreme conditions which occur at the center of a black hole. Using shock tube tests, we verified that this modification does not affect the treatment of shocks.

Furthermore, we improved the robustness of the conversion algorithm from evolved to primitive variables, allowing a clear distinction between physical and unphysical values. The details of this algorithm have already been described in [18]. For the current work, the only important aspect of the improvements is the ability to enforce a fine-grained error policy. The standard policy does not allow any unphysical values, with the exception of the internal energy falling below the zero temperature value (zero for the ideal gas EOS), in which case it is reset to that value. This can happen frequently when evolving cold matter, where the internal energy is exactly at the minimum value allowed by the given equation of state EOS. At densities corresponding to the surface region of the star, which is a notorious source of errors in hydrodynamic simulations, we use a more lenient policy, which adjusts unphysical values of the conserved energy and momentum densities to the physically meaningful range at a given density. The same applies to a region around the center of the black hole, which we define as the region in which $\alpha \leq \alpha_c = 0.1$ and which is always contained within the apparent horizon. In this region we also limit the Lorentz factor to be $W \leq 3$. This adjustment together with the aforementioned modified reconstruction allows us to evolve a black hole without excision for the spacetime or for the hydrodynamic variables.

Finally, we added an option to smoothly remove all matter from the center of a black hole. We do this to investigate how the presence of matter at the center of the black hole affects the numerical errors in comparison to an evolution of a vacuum black hole. This needs to be addressed separately from the spacetime-matter coupling elsewhere because, although our gauge is singularity avoiding, the gradients of

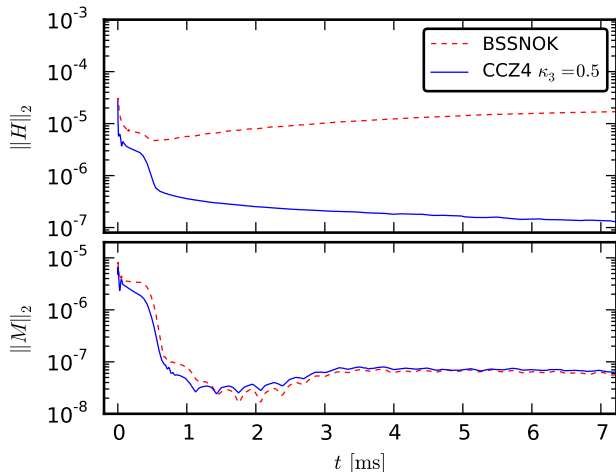


FIG. 1: Comparison of the CCZ4 and BSSNOK formulations in the evolution of a single and perturbed TOV star. The CCZ4 runs use parameters $\kappa_1 = 0.02$, $\kappa_2 = 0$. Shown are the L_2 norms of the Hamiltonian (top panel) and the combined momentum (bottom panel) constraint violations, taken over the full computational domain.

metric and density close to the center of a BH still become so large that it is always severely under-resolved numerically. To remove the matter, we introduce a term $-q/\tau_d$ to the RHS of the conserved variables $q = (D, \tau, S_i)$. The baryon mass then evolves according to $\dot{M}_b = -M_b/\tau_d$, thus leading to an exponential decay.

In simulations that form a black hole, we detect apparent horizons using the module `AHFinderDirect` [24] from the Einstein toolkit. We compute the mass and spin using the isolated horizon formalism [25, 26] implemented in the `QuasiLocalMeasures` module. Finally, the constraints equations (16)–(17) are computed using a standard 4th-order finite-difference method.

III. RESULTS

In this Section, we investigate the stability of the CCZ4 formulation when coupled to matter and test the convergence properties of the code. Furthermore, we compare the behavior of the constraint violations, first between the CCZ4 and the BSSNOK formulations, then between the CCZ4 and the Z4c formulations, and finally between the covariant and the non-covariant CCZ4 versions.

A. Isolated neutron star

For our first comparison, we choose an isolated spherically symmetric NS. The initial data obeys a polytropic EOS, *i.e.*, $P = K\rho^\Gamma$, with $\Gamma = 2$ and $K = 100$. During the evolution, we use a matching ideal gas EOS with $\Gamma = 2$. The star has a (gravitational) mass of $M = 1.4 M_\odot$ and a circumferential radius of $R = 14.16$ km. The grid setup can be found

in Table I.

In order to add a well defined initial constraint violation, we perturb the star with an eigenfunction of the $\ell = 2, m = 0$ fundamental mode in Cowling approximation. The amplitude we used corresponds to a radial velocity of 0.017 at the surface. Because a corresponding perturbation in the metric is not introduced, the Hamiltonian and momentum constraints are violated, in exactly the same way for CCZ4 and BSSNOK simulations.

When evolved in time, both formulations lead to stable solutions and the dynamics of the simulations agrees very well between BSSNOK and CCZ4, with a relative difference in the central rest-mass density that after 7.1 ms is only 3×10^{-4} . For comparison, the amplitude of the oscillations corresponds to a relative change of 0.015. The constraint violations are shown in Fig. 1. Since the components M^i of the momentum constraint are very similar, we show the combined norm

$\|M\|_2 \equiv \sqrt{\sum_i (\|M^i\|_2)^2}$. Clearly, the Hamiltonian constraint is damped efficiently by the CCZ4 formulation already after about 1 ms and is about two orders of magnitude smaller at the end of the simulation, *i.e.*, at $t \simeq 7$ ms. The BSSNOK formulation, on the other hand, exhibits a growth after a short initial decrease. In this setup, the momentum constraints are on average very similar for the CCZ4 and BSSNOK formulations.

Besides investigating the constraints, we also used this setup to test the convergence properties of the code. For this we used three different grid spacings, *i.e.*, $\Delta x = 443.0, 295.3, 196.9$ m on the finest level, differing by a factor 1.5, and evolved up to $t = 6.5$ ms. For the variables α, ρ , and γ , we then measured the convergence order as follows. First, we select the timesteps that are common to all resolutions. Next, we select the grid points on the finest refinement level which are present for each resolution. Then we compute for each variable and timestep the differences between the results for low and medium resolutions as well as medium and high resolutions. Finally, we compute the L_1, L_2 , and L_∞ norms of those differences over the selected grid points, and compute the time average of the norms. From those values we compute the convergence order n assuming the errors converge following a power law. We also compute the convergence order obtained at each time, which is shown in Fig. 2. For the lapse function, we find an overall convergence order of $n = 1.96, 2.07, 2.87$ for the L_1, L_2 and L_∞ norms, respectively, while for γ we obtain $n = 1.83, 1.98, 2.62$. For the rest-mass density ρ , on the other hand, we find $n = 1.45, 1.53, 1.85$.

The convergence order we would expect from the combined numerical schemes for spacetime and fluid in regions where fluid quantities are smooth and no fluid-vacuum boundary is present is two. However, the convergence of the hydrodynamic equations part is reduced near the surface of the star because of the use of an artificial atmosphere; furthermore, the convergence order also drops to one near shocks (although no global shocks are present in this test) and at local maxima. Because of these contaminations, the effective convergence order for the hydrodynamic equations is smaller, around $n \simeq 1.5$. On the other hand, the reason why the spacetime variables show better convergence in the given resolution range is prob-

simulation (stage)	h_0 [km]	h_f [km]	Levels	R_n [km]	R_{star} [km]	R_{BH} [km]	$M[M_\odot]$	symmetries
stable TOV	1.1814	0.2953	3 (0)	(94.5, 47.3, 23.6)	14.2	–	1.40	octant
unstable TOV	1.4746	0.1843	4 (0)	(118.0, 59.0, 29.5, 14.7)	8.59	–	1.44	octant
BH*	1.0220	0.1277	4 (0)	(81.7, 40.8, 20.4, 10.2)	–	2.36	1.00	octant
BH	1.4746	0.0921	5 (0)	(150.4, 82.6, 36.8, 18.4, 8.1)	–	2.36	1.00	octant
binary NS (inspiral)	9.4510	0.2953	6 (2)	(756.1, 354.4, 177.2, 94.5, 32.5, 16.2)	12.4	–	1.57	z and π
binary NS (merger)	9.4510	0.2953	6 (0)	(756.1, 354.4, 177.2, 94.5, 37.8, 21.6)	–	–	–	z and π
binary NS (collapse)	9.4510	0.1477	7 (0)	(756.1, 354.4, 177.2, 94.5, 37.8, 21.6, 10.8)	–	3.60	3.20	z and π

TABLE I: Grid setups of our simulations. Here, h_0 and h_f denote respectively the coarsest and finest grid spacing, R_n are the radii of each refinement level (in case of levels with moving boxes the radius of each box), R_{star} the initial neutron star coordinate radius, R_{BH} the coordinate radius of the final BH, if present, and M is the gravitational mass of the NS or of the BH. Note that the simulation BH* refers to a stationary BH evolved with a numerical domain with extents rescaled so that they match those of the collapsing star.

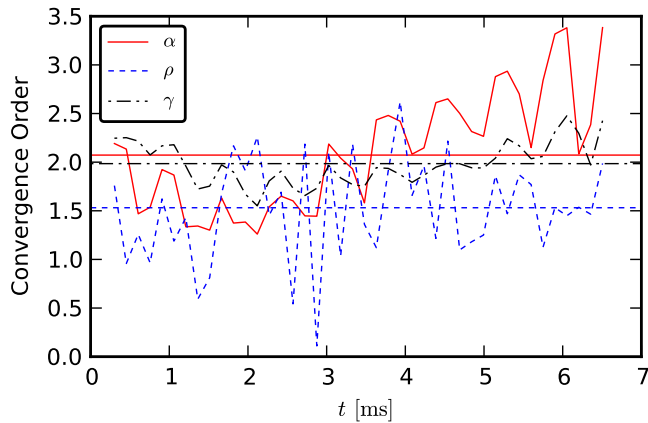


FIG. 2: Convergence test of the implementation of the CCZ4 formulation when coupled to the matter evolution and when using a stable perturbed TOV star. Shown is the time evolution of the convergence order obtained from the spatial L_2 -norms of the residuals. The horizontal lines show the overall order obtained from the time averaged residuals.

ably that the spacetime is mainly influenced by the bulk properties of the matter, which are less affected by the aforementioned problems. These results are in good agreement with what was found when analyzing the convergence order of the waveforms from binary NSs that we will discuss in Section III D (see also [27]).

B. Collapse to a black hole

Our next test consists of a NS on the unstable branch, to which we apply a small inwards velocity kick in order to trigger a collapse to a black hole. We use the same EOS as for the stable TOV test in the previous section, but the central density is $5 \times 10^{15} \text{ g cm}^{-3}$, the gravitational mass is $M = 1.44 M_\odot$, and the circumferential radius $R = 8.59 \text{ km}$. The velocity perturbation is simply given by $v^r = \mathcal{V}r/R$, with $\mathcal{V} = -0.01$. The purpose of this test is not only to compare the constraint violations between the CCZ4 and the BSSNOK formulations, but also to show that both formulations lead to a stable evolu-

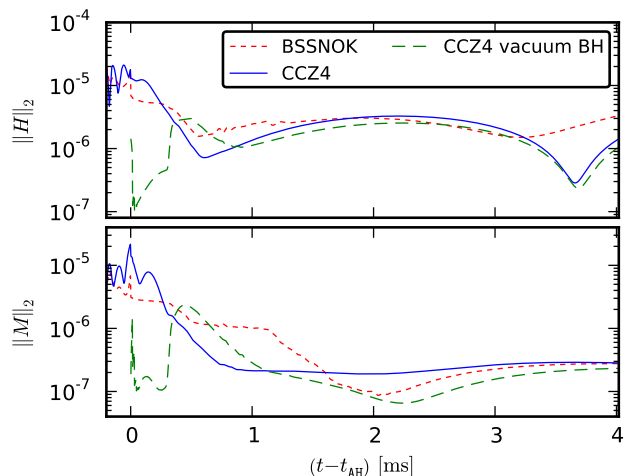


FIG. 3: Comparison of the CCZ4 and BSSNOK simulations for the collapse of an unstable TOV star to a BH. Shown are the L_2 norms of the Hamiltonian (top panel) and the momentum constraint violations (bottom panel), with the norms taken over the region outside the apparent horizon. The constraint violations are given in units $G = c = M_\odot = 1$. For comparison, we also show results for a pure vacuum CCZ4 simulation of a single Schwarzschild BH of the same mass as the NS model and using the same grid setup. The parameters for the CCZ4 simulations are $\kappa_1 = 0.065$, $\kappa_2 = 0$, $\kappa_3 = 0.5$. The time coordinate is relative to the time t_{AH} of apparent horizon formation.

tion of the black hole when coupled to matter.

We observed that the in-falling matter ends up in the central numerical cell. The matter then stays there, the relative change of total baryon mass between $t = 1.9 \text{ ms}$ (after the collapse) and 5 ms was less than 10^{-7} . The profile of lapse function, shift vector, density, and metric determinant all approach stationary values shortly after the BH has formed. Between 1.9 and 5 ms , the lapse function at the center changes by less than 3%. There is however a numerical instability in the fluid velocity inside the cell at the center of the BH, but since we limit the maximum velocity at the center of the BH as described in Section II, this quickly becomes stationary as well.

Type	Formulation	κ_1	κ_3	h_f/M	L/M	$\delta M/M$
BH	CCZ4	0.020	0.5	0.0625	102.0	0.16 %
BH	CCZ4*	0.020	1.0	0.0625	102.0	2.80 %
BH	CCZ4*	0.100	1.0	0.0625	102.0	0.10 %
BH	CCZ4	0.094	0.5	0.0866	55.4	0.76 %
BH	Z4c	0.020	–	0.0625	102.0	0.03 %
collapse	BSSNOK	–	–	0.0866	55.4	0.03 %
collapse	CCZ4*	0.100	1.0	0.0866	55.4	1.01 %
collapse	CCZ4*	0.170	1.0	0.0866	55.4	0.23 %
collapse	CCZ4	0.020	0.5	0.0866	55.4	2.09 %
collapse	CCZ4	0.100	0.5	0.0866	55.4	2.21 %
collapse	CCZ4*	0.100	0.5	0.0866	55.4	0.51 %
collapse	Z4c	0.020	–	0.0866	55.4	0.16 %

TABLE II: Accuracy of the BH mass for simulations of nonrotating vacuum BHs and BHs created by the collapse of unstable spherical NSs. Note that the simulations marked with * use the prescription (27) for the damping coefficient κ_1 , in particular those performed with the fully covariant formulation, *i.e.*, with $\kappa_3 = 1$. The maximum deviation of the measured BH mass from the exact value during the first 800 M after the detection of the apparent horizon is denoted by δM . For the collapse simulations, the time up to 200 M after BH formation is ignored. L is the position of the outer boundary, and h_f the grid spacing on the finest level.

The evolution of the constraints is shown in Fig. 3. For comparison, we evolved a Schwarzschild BH of the same mass using the CCZ4 spacetime evolution code without the fluid part, but with the same grid setup. As shown in Fig. 3, the constraint violations are very similar to the collapse simulation after the BH has formed. The L_2 -norms excluding the BH interior agree very well not only in magnitude but also in terms of the long time behavior.

The norms including the BH interior (not shown in the plot) for vacuum BH and collapse agree very well initially. However, when the aforementioned instability develops during the evolution with matter, the norm of the momentum constraint is increased by a factor ≈ 2 . In order to determine whether this affects the exterior of the BH, we conducted a numerical experiment. Directly after the formation of the BH, we introduced a source term to the fluid variables as described in Section II C in order to exponentially remove the matter over an e-folding timescale $\tau_d = 0.025$ ms. This source term is only active near the center of the BH, which we define for simplicity via the lapse function by the condition $\alpha < 0.007$. The instability at the center of the BH and the corresponding jump in the momentum constraint do not occur anymore when using this method. However, there is no visible change of the norm of the constraint violations outside the BH.

We conclude that the constraint violations outside the BH are not influenced significantly by the presence of matter inside the BH. The coupling of the hydrodynamic evolution to the spacetime evolution with the CCZ4 method does not seem to compromise the stability of the BH evolution in any way. It is however necessary to either limit the fluid state at the center of the BH as described in Section II or to gradually remove

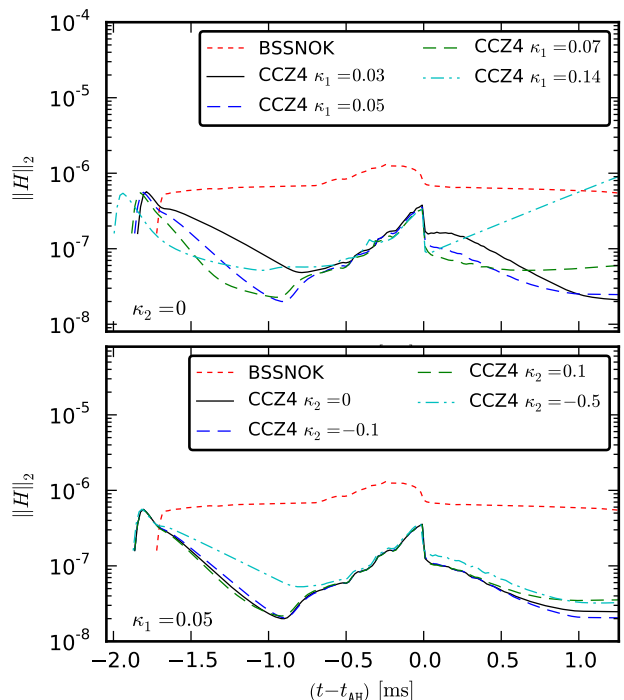


FIG. 4: Comparison of the Hamiltonian constraint violations when evolving the eccentric binary using the CCZ4 system with different parameters, and with the BSSNOK system. *Top panel:* Influence of parameter κ_1 , keeping $\kappa_2 = 0$, $\kappa_3 = 0.5$ fixed. *Bottom panel:* Influence of parameter κ_2 , keeping $\kappa_1 = 0.05$, $\kappa_3 = 0.5$ fixed. Shown is the time evolution of the L_2 -norm of the Hamiltonian constraint, excluding the interior of the apparent horizon.

the matter from the center as described above.

As a measure of accuracy, we monitor the BH mass extracted using the isolated horizon formalism. For the collapse of a spherical star, the BH has to be stationary after all matter crossed the horizon, and the BH mass has to be exactly the ADM mass of the initial unstable star. We therefore compute the maximum deviation of the numerically extracted value from the exact one during the time interval 200–800 M after apparent horizon detection. The results are reported in Table II. For the non-covariant CCZ4 simulations of the collapse, the accuracy is around 2.1–2.2 % for damping parameters $\kappa_1 = 0.1, 0.02$. As we will show in Section III F, the error can be reduced further by a modification of the damping terms, which allows the use of the fully covariant version. Nevertheless, the standard BSSNOK formulation is more accurate in terms of BH mass for this test.

C. Binary neutron stars with constraint-violating initial data

We next present tests of the CCZ4 formulation when applied to merging binary NSs with constraint-violating initial data. These are probably the most demanding tests with respect to constraint violations because the initial data already contains large violations of the constraint equations.

We start by considering binaries on eccentric orbits and set up such initial data by starting with a constraint-satisfying solution representing an irrotational binary on a quasi-circular orbit and then simply scale the velocity by a factor 0.85 to make the orbit eccentric (which also speeds up the inspiral). This naturally introduces a large constraint violation, thus allowing us to compare the evolution schemes under extreme but well-defined conditions. More specifically, the original initial data represents an irrotational binary system on a quasi-circular orbit, with equal baryon masses of $M_b = 1.779 M_\odot$, and an initial separation of $d = 45$ km. The stars obey a polytropic EOS with $\Gamma = 2$ and $K = 123.629$, while during the evolution we use an ideal gas EOS with $\Gamma = 2$. This model is publicly available from the `LORENE` code.

We evolve the eccentric system with the CCZ4 formulation, using various combinations of the parameters, as well as with the BSSNOK formulation. The rest of the setup stays exactly the same, in particular the gauge conditions. Figure 4 shows the evolution of the Hamiltonian constraint. As one can see, the constraint violations, which are the same initially, are reduced by up to one order of magnitude during the inspiral when using the CCZ4 formulation. The BSSNOK formulation, on the other hand, shows a moderate growth during the inspiral. Of course the impact of the initial constraint violation on the actual dynamics of the binary is difficult to assess. Any constraint violation is obviously a deviation from the solution of the Einstein equations, although the quantitative relation between the constraint violations and the error on the physical quantities is largely unknown. It is however reasonable to assume that a reduction of constraint violations will also lead to more accurate results for the physical quantities. In this respect, the CCZ4 formulation is clearly better for the case considered here. Note that the accuracy that can be achieved in this way is still limited by the constraint-satisfying component of the evolution error, so that a further reduction will not increase significantly the overall accuracy.

In order to assess how the constraint violation influences the orbital motion we have compared the trajectories of the two NSs obtained with the CCZ4 and BSSNOK formulations by tracking the “barycenters” of the two NSs¹. We find that significant deviations between the two trajectories develop during the evolution while simultaneously also the differences in the constraint violations grow. After one orbit, the coordinate separation already differs by 18 %. This is to be expected. Once the constraints are violated, the numerical solution of our evolution system belongs to an extended set of solutions of the Einstein equations. Even starting with the same amount of constraint violation, the evolution equations for CCZ4 and BSSNOK formulations are expected to lead to slightly different results, in the vicinity of the true Einstein solution. The only question is below which magnitude of the constraint vi-

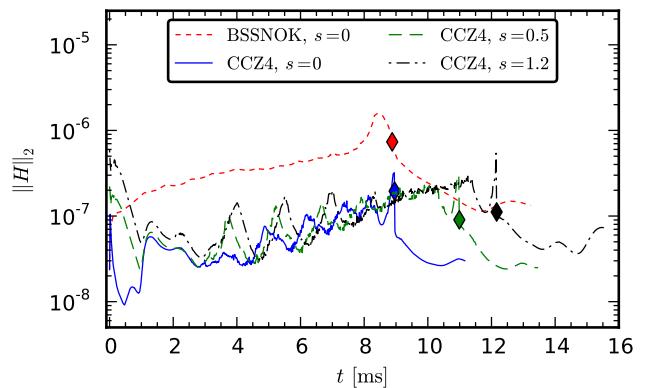


FIG. 5: Evolution of the Hamiltonian constraint during mergers of spinning binary NSs on quasi-circular orbits, where the spin was added to the initial data in a constraint violating way. Shown are results obtained with the CCZ4 formulation for various amounts of spin. For the irrotational model, also the results of the BSSNOK formulation are shown.

olation the errors become tolerable. Clearly, the constraint violation introduced by the crude rescaling of the velocity is already too large to obtain meaningful results.

When comparing simulations with CCZ4 using different parameters, we find that increasing the damping parameter κ_1 leads to a decrease the violations of the Hamiltonian constraint during the inspiral phase. This is indeed what one would naively expect given that a larger κ_1 amounts to a smaller timescale for the damping of the constraint violations. However, for $\kappa_1 \lesssim 0.07$, we find an exponential growth after the BH has formed, signalling that the constraint damping action is no longer effective. Hence, the optimal choice for a stable evolution seems to be $\kappa_1 = 0.05$. So far, we used a damping parameter $\kappa_2 = 0$. We did not find any significant improvement by trying different values. On the contrary, for $\kappa_2 = -0.5$ the constraint damping becomes less efficient.

Next, we consider mergers of rotating NSs. Because self-consistent initial data for rotating NS binaries is not available, (although an approach to compute such models has been proposed recently in Ref. [28]), we will show in the following that it is possible to use a short evolution with the CCZ4 scheme to convert constraint-violating initial data into self-consistent initial data. This allowed us to study the influence of the additional NS spins on the spin of the final BH and the surrounding disk. Although some of these results have already been presented in Ref. [29], for completeness, we review here the behavior of the two formulations in this illustrative test.

The models we investigate are constructed in a similar way as for the eccentric case, namely, by starting from irrotational quasi-circular initial data. The spin is added by simply rescaling the velocity field in the co-orbiting frame by a factor $1 - s$, where $s = 0$ corresponds to the original irrotational model, and $s = 1$ roughly to the corotating one (see [29] for details). Naturally, this introduces constraint violations, which are however not as strong as for the eccentric binary. It also causes ordinary oscillations of the star, which affect only the realism of the initial conditions and are not important within

¹ We define the position of the “barycenter” of each NS simply as an extension of the Newtonian expression, *i.e.*, $(\int_V \hat{D}x^i d^3x) (\int_V \hat{D} d^3x)^{-1}$, where the integration volume V is suitably chosen to fully contain the selected NS, but exclude the other.

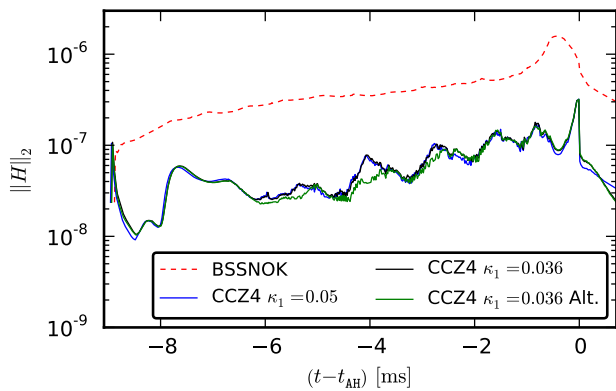


FIG. 6: Comparison of the Hamiltonian constraint violations when evolving with BSSNOK and CCZ4 system, for the quasi-circular coalescence. Shown is the time evolution of the L_2 -norm of the Hamiltonian, excluding the interior of the apparent horizon. For CCZ4 we show results obtained with $\kappa_1 = 0.05$, $\kappa_1 = 0.036$, and $\kappa_1 = 0.0036$ using an alternative grid structure (“Alt.”) which contains moving boxes only on the finest level. All CCZ4 runs were carried out with $\kappa_2 = 0$, $\kappa_3 = 0.5$.

the scopes of this test.

The spatial distribution of the constraint violation shown in [29] is similar to the one shown in Fig. 7, only the initial constraint violation is more pronounced. Figure 5 shows the evolution of the Hamiltonian constraint for various amounts of the spin. The increase of the initial constraint violation with the spin is clearly visible. However, even for the fastest-spinning model, the evolution with the CCZ4 formulation rapidly reduces the Hamiltonian constraint to a much smaller magnitude, which already after ~ 1 ms becomes comparable with the one obtained with the BSSNOK formulation when evolving constraint-satisfying initial data. As we will show in Section III D, the amount of constraint violations for the latter are tolerable. We thus conclude that at these separations an evolution time of ~ 1 ms with the CCZ4 formulation is sufficient to produce initial data that can be considered self-consistent. Of course, although self-consistent, the initial data may well represent a physical system which is rather different from the intended one.

D. Binary neutron stars with constraint-satisfying initial data

We now turn to investigate the behavior of merging binary NSs in quasi-circular orbits. For this, we evolve the original binary star model described in the previous subsection, without reducing the linear momenta. Again, we find that the CCZ4 formulation suppresses the Hamiltonian constraint by roughly one order of magnitude when compared to the BSSNOK formalism, as shown in Fig. 6. Varying the damping constant κ_1 in the stable range impacts the results only marginally. Figure 6 also shows a clear periodic increase/decrease of the Hamiltonian constraint violation when using the CCZ4 formulation. We believe that this behavior is related to the movement of the refined boxes. Whenever a re-

fining box moves, the new points have to be computed by interpolation from the coarser grid, which introduces an additional error. Indeed, the period of the variations in the constraint violations corresponds to half an orbit, which is compatible with the π -symmetry of the binary. However, to further validate this hypothesis, we performed a simulation where only the finest level consists of moving boxes, in contrast to the standard setup where the two finest levels are moving boxes. As one can see in Fig. 6 by comparing the solid black and green lines, this has some influence during inspiral. Moreover, it is most prominent at the stage where the change of the overlap of the moving boxes on the second finest level is also large. The fact that we do not observe the periodic pattern for the BSSNOK results seems to indicate that the error due to regridding is not dominant in this case.

Since binary NS mergers are an important application of our code, we performed a computationally expensive convergence test with three resolutions, each increased by a factor of 1.5. We measure the convergence order by the same method used for the single star, only that we use the finest non-moving refinement level instead of the finest one. Furthermore, we exclude the interior of the apparent horizon (more precisely, we exclude a coordinate sphere with the mean coordinate radius of the horizon). For the lapse function we measure an overall convergence order of $n = 1.9$, while for the rest-mass density this is $n = 1.6$, all measured using the L_2 -norm. The metric determinant γ develops a strong peak at the center of the grid shortly before the apparent horizon forms. This is normal, but complicates measuring the convergence after BH formation. Indeed, during the inspiral, we obtain a convergence order $n = 1.7$ for γ , which is recovered again after the BH formation. We note that the time dependent estimate for the convergence order of all variables fluctuates strongly during the merger (up to $n = 8$), which is probably caused by the accumulated phase error. As a consequence, we cannot prove convergence for this stage. We can however establish convergence of the end result, *i.e.*, of the final BH, which should be insensitive to the phase error. To this end, we compared the final mass and spin of the BH as well as the time until apparent horizon formation.

As reported in Table III, we find a convergence order around 1.2 for the BH properties. This is not surprising since the convergence order of the hydrodynamic evolution scheme probably reduces to one during the merger due to the formation of strong shocks. Nevertheless, the errors of BH mass and spin are quite small. Using Richardson extrapolation, we obtain an extrapolated total error for the values obtained at the lowest resolution which is 0.9 % for the BH mass and 0.3 % for the spin. The appearance of an apparent horizon is the result of an independent search algorithm on a complex combination of the evolved quantities and, as such, not necessarily sharing the same convergence order of the evolved equations. That said, we find that the time of first appearance of an apparent horizon has a convergence order $n = 2.1$, but is also the quantity with the largest error. The error with respect to the Richardson extrapolated time is 9 % for the lowest resolution and 2 % for the highest. The error introduced by the different frequency at which the apparent horizon is searched at different resolutions

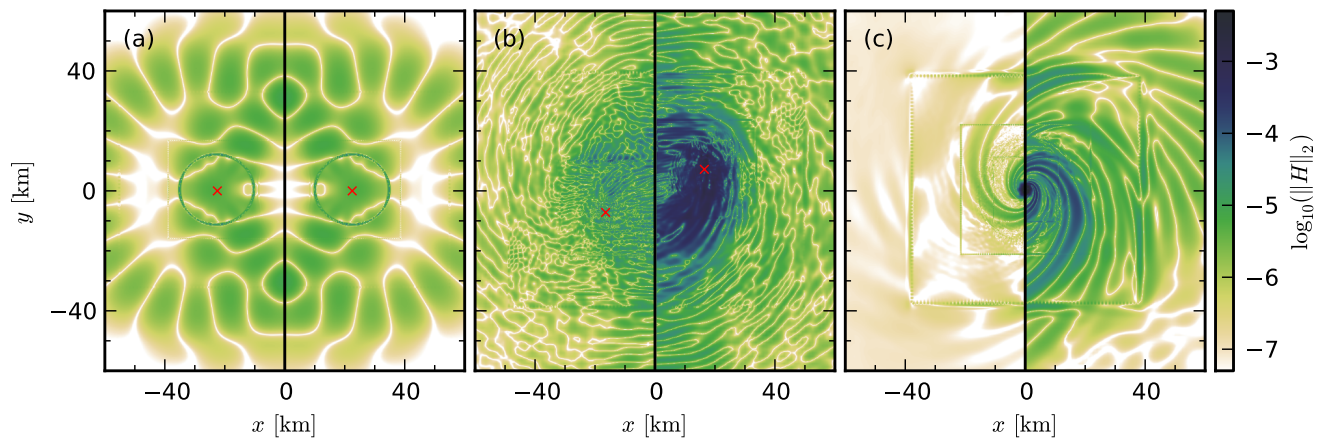


FIG. 7: Comparison of the local Hamiltonian constraint violations when evolving the quasi-circular coalescence with the BSSNOK and CCZ4 systems. The panels depict the Hamiltonian constraint in the (x, y) plane at different times: (a) $t = 0$, initial data, (b) $t = 6$ ms, inspiral, (c) $t = 12$ ms, final state. The left half of each panel shows the CCZ4 results, the right half the BSSNOK results. The locations of the NS barycenters are marked by the red crosses.

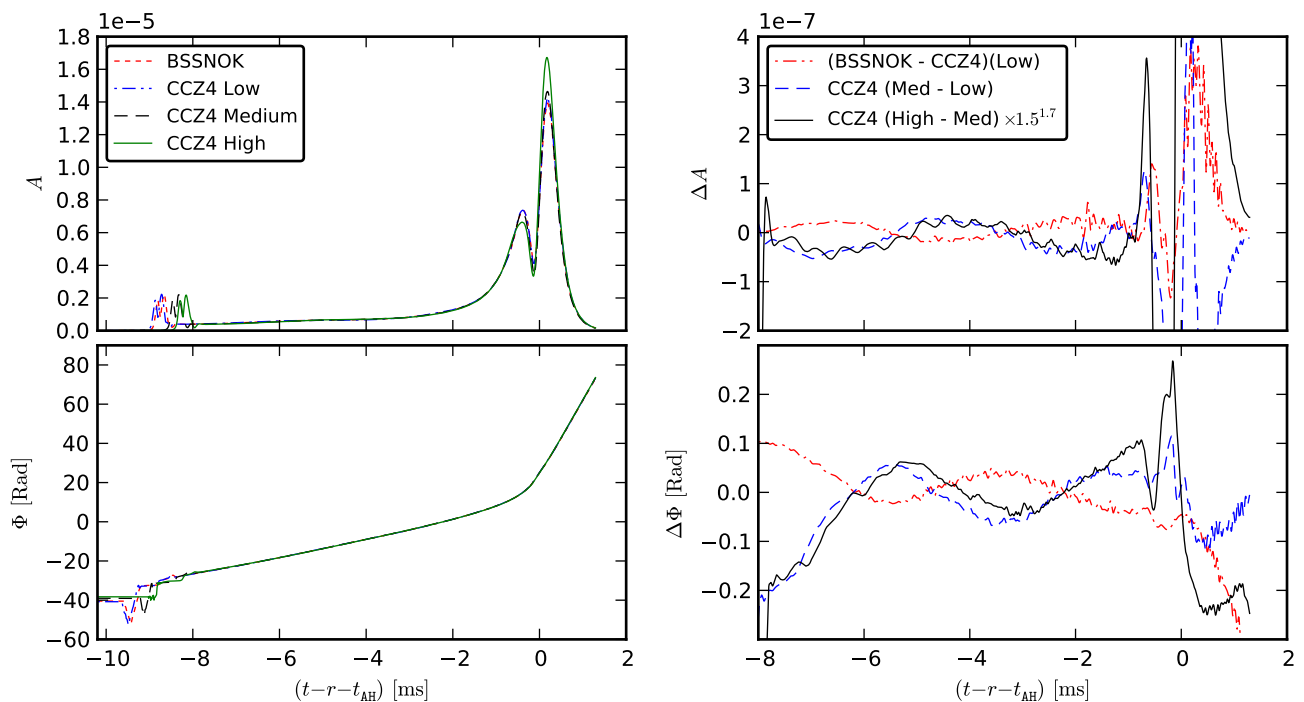


FIG. 8: Accuracy of the gravitational wave signal in terms of the $\ell = m = 2$ multipole component of the Weyl scalar Ψ_4 , extracted at $r = 664$ km. *Top left*: Amplitude of Ψ_4 . *Bottom left*: complex phase Φ (see main text). *Top right*: Residuals of the amplitude between CCZ4 simulations with different resolutions, and between BSSNOK and CCZ4 at lowest resolution. The residual between high and medium resolution is rescaled assuming a convergence order of 1.7. *Bottom right*: Residuals of the phase, also rescaled.

is much smaller and only $\sim 0.1\%$.

In contrast to the eccentric case, the dynamics of the quasi-circular system agrees well between the CCZ4 and BSSNOK formulations. To quantify this statement, we compare mass, spin, and formation time of the BH in Table III. The agreement is better than 1%. The differences in the BH properties are thus comparable to the numerical errors of the CCZ4 simulation as determined by the convergence test. Curiously,

the difference in horizon formation time is an order of magnitude smaller than the numerical errors for this particular case, although we do not expect that this holds in general. Since the constraint violations still differ by a factor ≈ 10 between CCZ4 and BSSNOK, one can conclude that the magnitude of constraint violations observed in the quasi-circular BSSNOK evolution is tolerable, while the amount present in the eccentric case already leads to severe errors. This is very use-

	BSSNOK	CCZ4	Δ_{Form}	Δ_{Res}	n
M_{BH}/M_{\odot}	3.222	3.204	0.6 %	0.5 %	1.2
a_{BH}	0.837	0.840	0.4 %	0.2 %	1.2
t_{BH} [ms]	8.88	8.94	0.7 %	7.0 %	2.1

TABLE III: Comparison of physical quantities at the end of the quasi-circular coalescence, obtained with the BSSNOK and CCZ4 formulations. Above, M_{BH} is the mass of the final BH, $a_{\text{BH}} = J_{\text{BH}}/M_{\text{BH}}^2$ its dimensionless spin parameter, and t_{BH} is the time when the apparent horizon is detected. The difference between the highest and lowest resolution of the CCZ4 convergence test is given by Δ_{Res} , while p is the measured convergence order. The difference between results obtained with the BSSNOK and CCZ4 formulations at the lowest resolution is denoted by Δ_{Form} .

ful notion since, as we discussed before, the relation between constraint violation and error of physical quantities is largely unknown. We stress that the L_2 -norm we use to quantify the constraint violations depends on the computational volume and the falloff behavior of the constraint violations. For different setups, one has to rescale accordingly in order to make sensible comparisons.

Besides the amount of constraint violation, we are also interested in its spatial distribution. Figure 7 shows the Hamiltonian on a cut in the (x, y) plane. Clearly, most of the violations are produced along the orbit of the stars. Also the mesh refinement boundaries are clearly visible. In practice, the stars leave behind a trail of constraint violations, which is more pronounced and decays more slowly for the BSSNOK formulation. Furthermore, constraint violations travel through the computational domain and are partially reflected at each refinement boundary, both for the CCZ4 and the BSSNOK formulations. After the formation of the BH, when the system approaches a final state, the constraints exhibit a relatively stationary spiral pattern of slowly decreasing magnitude.

Finally, we should also remark that the relative difference in the constraint violations that we measure in the simulations reported here refers to *our* implementation of the CCZ4 and BSSNOK formulations and should not be considered as universal. Because a number of slightly different versions of the BSSNOK system are used by different groups, it is possible that the differences between the two formulations could also be smaller or larger when performed by other groups.

1. Gravitational-wave signal

One of the most important results of binary NS merger simulations are obviously the gravitational-wave (GW) signals. Since prior to extraction, GWs travel into the weak field region, crossing several refinement boundaries and become a small perturbation due to the $1/r$ falloff, they might be affected more strongly by numerical errors than the bulk dynamics of the merger. In particular, constraint violations could affect the GWs differently. In the following, we measure the numerical accuracy of the GW signal using the CCZ4 conver-

gence test, and estimate the influence of constraint violations by comparing between the CCZ4 and the BSSNOK formulations.

For this, we extract the $\ell = m = 2$ component of the Weyl scalar Ψ_4 at a fixed radius $r = 664$ km. We then decompose the complex quantity Ψ_4 into amplitude and phase, *i.e.*, $\Psi_4 = A \exp(i\phi)$, where ϕ is a continuous function of time. To compare different simulations, we measure time with respect to the time t_{AH} at which the apparent horizon forms, and introduce the phase difference $\Phi(t) = \phi(t) - \phi(t_{\text{AH}})$. The amplitude and the phase are shown in the left panels of Fig. 8 for the BSSNOK and CCZ4 results. For the CCZ4 simulations, we plot the three resolutions of the convergence test, where the lowest one is identical to the one used for the BSSNOK simulation. One can clearly distinguish the inspiral phase, a first peak corresponding to the merger, and a second peak corresponding to the ringdown of the BH. The usual junk radiation inherent to the initial data can also be seen at the beginning of the evolution. In the right panels of Fig. 8, we show the residuals of amplitude and phase between different resolutions and between the CCZ4 and BSSNOK runs when performed at the lowest resolution. For the CCZ4 runs we find errors compatible with a convergence order around 1.7 during the inspiral. During the merger on the other hand, the convergence decreases and is lost during the ringdown phase. From the time derivative of Φ , we compute the instantaneous frequency, which increases from around $\dot{\Phi} \approx 7$ rad ms⁻¹ at the end of the inspiral to $\dot{\Phi} \approx 35$ rad ms⁻¹ at the maximum of the ringdown signal. Unfortunately, the wavelength corresponding to the latter is resolved by only 6 coarsest grid points of the lowest resolution, and thus the signal from the ringdown is severely under-resolved. In order to demonstrate convergence of the high-frequency part of the signal, we would have to repeat the runs with much higher resolution in the weak field region.

In the analysis of GW data using matched filtering techniques, the most important error is the phase shift during the inspiral. For our test case, we find that the total phase error until merger is less than 0.4 rad for the lowest resolution, and 0.1 rad for the highest one. At first sight, this seems to contradict the larger relative error we obtain for the time until BH formation (compare Table III). However, by analyzing the coordinate separation² of the stars barycenter, we found that the relative error of separation is larger than the error of the GW phase, *i.e.*, the orbital period is more accurate than the decrease in separation per orbit. This is reflected in the relatively large amplitude error (see Fig. 8), since the GWs at the same phase (or time) are produced at different orbital separations.

Figure 8 also shows that the differences in the waveforms obtained with the CCZ4 and the BSSNOK formulations are generally comparable to the numerical errors, even during merger and ringdown. Since the constraint violations differ

² Note that although the gauge condition is the same for both simulations, the coordinate separation is a gauge dependent quantity.

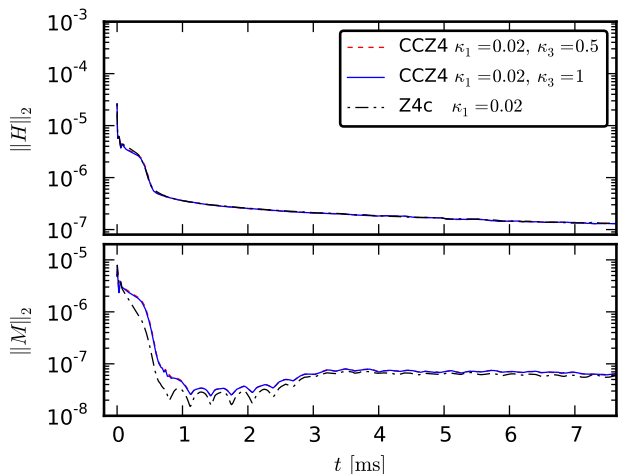


FIG. 9: Comparison between the non-covariant and covariant CCZ4 and the non-covariant Z4c systems in evolutions of a non-rotating stable neutron star. Shown is the time evolution of the L_2 -norm of the Hamiltonian constraint violation (top panel) and the momentum constraint violation (bottom panel).

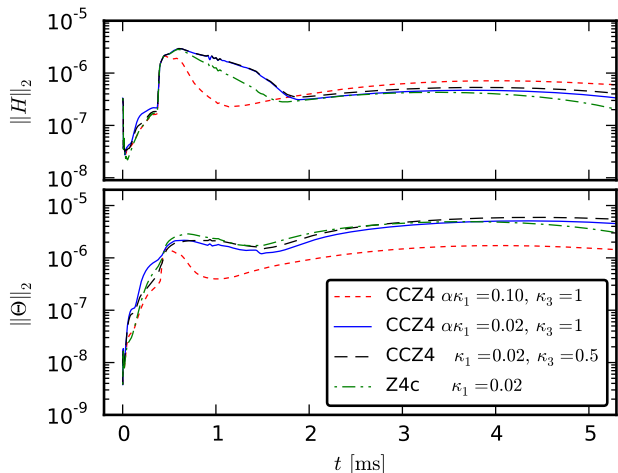


FIG. 10: Comparison between the non-covariant and covariant versions of the CCZ4 and the non-covariant Z4c systems in evolutions of a non-rotating BH. Shown is the time evolution of the L_2 -norm of the Hamiltonian constraint violation (top panel) and of the Θ variable (bottom panel), computed excluding the interior of the BH.

by one order of magnitude, we can conclude that their impact on the GW signal is also comparable to the one due to ordinary numerical errors, or even smaller (the differences could as well be purely due to numerical errors other than the constraint violation). This result is rather reassuring since, to the best of our knowledge, the impact of the constraint violations on the accuracy GW signal has not been measured before.

E. Comparison with the Z4c formulation

As anticipated in the Introduction, we now present a comparison of the results obtained with another conformal formulation of the Z4 system, namely the Z4c formulation proposed in Ref. [11]. To reduce the computational costs, the comparison will be carried out with the evolutions of a stable non-rotating star, of a single non-rotating BH and of an unstable NS which collapses to a BH. However, we expect that the qualitative behavior of the two formulations will extend also to binary systems either of BHs or of NSs. As far as the Z4c system is concerned, we have implemented the formulation described in [11] within the `McLachlan` code [20]. This required only minor modifications in the source terms of the CCZ4 system (see Section II A for details about the differences between the two systems). We also use the radiative boundary conditions provided by the `McLachlan` code, initially developed and well-tested for the BSSNOK system.

We note that both the CCZ4 and the Z4c formulations implement the same constraint-damping scheme [12] and we use the values of the constraint-damping parameters advocated as best suited for the Z4c formulation in Ref. [11], namely, $\kappa_1 = 0.02$ and $\kappa_2 = 0.0$. Also, for both systems we monitor the same quantities, namely, the behavior of the Hamiltonian and momentum constraint violations, but also of the Θ function, whose time variation measures the size of the Hamiltonian-constraint violation and thus assesses the deviation of the numerical solution from the true Einstein solution. Indeed, we find this diagnostic quantity a very important indicator of the quality of the solution, which can be compared directly for the two conformal formulations (we recall that the Θ function is not defined for the BSSNOK formulation).

The first test involves a non-rotating stable NS, as described in Section III A. Overall, in the presence of matter the two systems provide an almost identical behavior and show two orders of magnitude decrease in the constraint violations as the evolution is started. These are reported in Fig. 9, which shows both the violations in the Hamiltonian and the momentum constraints (top and bottom panels, respectively).

The second test involves the evolution in vacuum of a non-rotating BH. The results are again very similar for the two systems, as one can see in Fig. 10, which reports the violation in the Hamiltonian constraint and the evolution of the Θ function (top and bottom panels, respectively). Note that while the Hamiltonian constraint is slightly smaller for the Z4c formulation, the momentum constraint is smaller for CCZ4. Both systems show small deviations in the final BH mass, see Table II.

The third comparative test consists in the collapse of an unstable TOV star, as described in Section III B. Figure 11 shows again the violation in the Hamiltonian constraint and the evolution of the Θ function (top and bottom panels, respectively). The only significant difference in this case is a spike in the CCZ4 formulation right after collapse, which is efficiently damped after 1 ms of evolution, so that the constraint violations return to values similar to the Z4c formulation. The value of the BH mass after collapse shows larger errors for CCZ4, around 2.09%, in comparison with only 0.16% for Z4c

(see Table II). However this result can be improved to 0.51% error by using a modified damping scheme with $\kappa_1 = 0.1$ (see Section III F).

Based on the results presented above, we conclude that the CCZ4 and the Z4c formulations yield very similar results in terms their ability to damp the violations in the constraint equations. However, one important difference remains between the two systems, that is, only the CCZ4 formulation (*i.e.*, with $\kappa_3 = 1$) represents a version of the original Z4 system that is not only conformal but also *covariant*. As a result, only for this covariant formulation one should reasonably expect that the qualitative behavior of the constraint violations will remain unchanged when evolving the same system in different coordinates. Finally, given the similar behavior of the CCZ4 and of the Z4c formulations for the tests considered here, we expect that, when used in the evolution of binary NSs, also the Z4c system would yield violations that are of about one order of magnitude smaller than those with the BSSNOK formulation.

F. Fully covariant CCZ4 in black-hole spacetimes

As a concluding Section, we now discuss how it is possible to employ a fully covariant CCZ4 formulation, *i.e.*, with $\kappa_3 = 1$, also for spacetimes containing BH singularities. We recall that in cases where no singularity is present, as for example in the evolution of a TOV, the fully covariant CCZ4 system is stable and the standard constraint damping prescription leads to results similar to the non-covariant CCZ4 formulation as well as to the Z4c systems (*cf.* Fig. 9). However, in those cases in which a BH is present, either initially or when it is formed during the evolution, the fully covariant CCZ4 system coupled with the constraint damping scheme has shown exponentially growing modes (*cf.* Fig. 4 in paper I).

Even though we could not identify the exact cause of the instability (see discussion in Section II A), it is clear that in Eqs. (4) and (5) the *constant* damping coefficient κ_1 is always multiplied by the lapse function α . Because our singularity-avoiding slicing reduces considerably the value of the lapse near the singularity, it is clear that the benefits introduced by the damping term κ_1 are severely suppressed right there where the violations are the largest. Fortunately, these considerations suggest two new prescriptions for the damping terms, namely

$$\kappa_1 \rightarrow \frac{\kappa_1}{\alpha}, \quad (27)$$

$$\kappa_1 \rightarrow \frac{\kappa_1}{2} \left(\alpha + \frac{1}{\alpha} \right), \quad (28)$$

thus transforming κ_1 from a constant function to a spatially varying one. More importantly, the product $\alpha\kappa_1$ is not approaching zero anymore near the singularity. Although the two prescriptions (27) and (28) are slightly different in their local and asymptotic behavior, they yield very similar results.

To validate the effectiveness of the new prescription, and in particular of the form (27), we recompute the tests performed in the previous Section and compared them with those

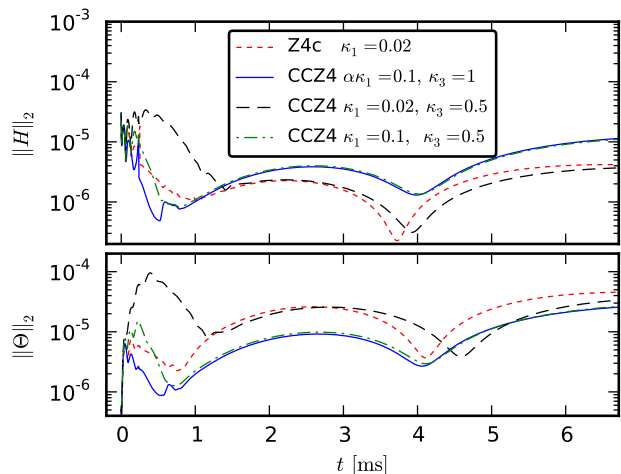


FIG. 11: Comparison between the non-covariant and covariant versions of the CCZ4 and the non-covariant Z4c systems in evolutions of an unstable TOV star collapsing to a BH. Shown is the time evolution of the L_2 -norm of the Hamiltonian constraint violation (top panel) and of the Θ variable (bottom panel), computed excluding the interior of the BH.

obtained with the non-covariant version of the CCZ4 formulation (*i.e.*, with $\kappa_3 = 0.5$) and with the Z4c formulations. Since we use the same computational infrastructure, numerical methods and gauge conditions, the only difference between the two systems are the Z4 source terms which were truncated in the non-covariant CCZ4 version and are completely removed in the Z4c system (see Eqs. (1)-(6)).

The comparison is shown in Fig. 10, which presents results obtained with two values of the damping parameter, namely $\kappa_1 = 0.1$ and $\kappa_1 = 0.02$, in evolutions of a single non-rotating BH. The latter allows a direct comparison with the non-covariant CCZ4 and Z4c results, and indeed the constraint violations are very similar in this case. Larger damping values lead to lower values of Θ and of the violations of the momentum constraints. Even though the two damping parameters are significantly different, the violations of the constraints change by less than one order of magnitude over the timescale of this evolution, *i.e.*, 5 ms. A significant effect however is observed in the black hole mass, which shows deviations of 0.1% in the first case and 2.8% in the second case (see Table II).

Overall, the behavior of the fully covariant CCZ4 constraints matches well the non-covariant version of the CCZ4 system for the same value of the damping parameter, for example $\kappa_1 = 0.1$ in Fig. 11. However, the two versions of the CCZ4 formulations differ in the value of the final BH mass after collapse, namely, the covariant one shows a difference of 1.01% with respect to the initial gravitational mass of the NS, while the non-covariant one shows a 0.51% error. A study of the influence of different damping parameters on the values of the BH mass is presented in Table II. In practice, larger values of the damping lead to more reliable estimates of the mass, for example $\kappa_1 = 0.17$ reduces the error to 0.23%.

We believe that the new prescriptions for the damping term

(27) and (28) are important for two distinct reasons. First, they allow for the use of a fully covariant CCZ4 formulation also in singular BH spacetimes. This was a limitation of our approach in paper I that has been successfully overcome. Second, these results shed some light on the behavior of the “non-principal part” constraint-damping terms in the CCZ4 system, although a complete and closer comparison with the Z4c results presented in [11] cannot be performed because of the different boundary conditions employed.

IV. CONCLUSIONS

We have compared numerically the performance of several conformal and traceless formulations of the Z4 system with the BSSNOK formulation in simulations of spacetimes with and without matter, in terms of suppression of constraint violations and their impact on the accuracy of physical quantities. Besides coupling the CCZ4 system presented in paper I to matter sources, we have improved the fully covariant version of CCZ4 by modifying the κ_1 damping term, thus eliminating instabilities found when evolving BHs. In addition, we implemented the Z4c formulation described in [11] in our numerical framework and compared its properties to those of the CCZ4 formulation.

We have found that the non-covariant CCZ4 formulation is stable when coupled to matter sources in simulations of stable and unstable spherical NSs, as well as of merging binary NSs. In comparison to the BSSNOK system, the CCZ4 formulation reduces the constraint violations by one order of magnitude for simulations of binary NSs and by two orders for single NSs. We have also demonstrated the convergence of our implementation for simulations of stable NSs, as well as of binary NS mergers, with a convergence order in the range 1.2–2, mainly limited by the hydrodynamic evolution scheme. By comparing the CCZ4 and the BSSNOK evolutions and by using the large differences in the constraint violations, we could estimate the influence of the latter on physical quantities. In particular, we could demonstrate that the impact of the constraint violations on the GW signal from the binary NS mergers is smaller or comparable to the numerical errors.

Furthermore, a comparison of the different conformal Z4 versions, namely the non-covariant and covariant CCZ4 formulations, and the non-covariant Z4c, has shown that they have an almost identical behavior in terms of constraint violations as long as no singularity is present (*e.g.*, stable TOV). In evolutions of BH spacetimes or when a BH is produced as a result of a collapse, we find that values of the constraint damping parameter larger than the ones proposed for the Z4c formulation (*i.e.*, $\kappa_1 = 0.1$ in place of $\kappa_1 = 0.02$), lead to lower constraint violations and do not produce late-time instabilities. Finally, we have also found that the modification of the damping terms mentioned above is useful not only for a stable evolution of the full covariant CCZ4 system, but also for reducing the drift in the BH mass for both CCZ4 versions.

Overall, we recommend CCZ4 as the standard formulation of the Einstein equations to be used in numerical-relativity evolutions. In cases where constraint violations are problematic, *e.g.*, when using constraint-violating initial data, the CCZ4 formulation is clearly superior. On the other hand, when using constraint-satisfying initial data, the reduction of constraint violations is accompanied by errors that are very similar to those obtained with the BSSNOK formulation. No additional computational costs are needed and simple Sommerfeld radiative boundary conditions are sufficient to obtain stable evolutions. Of course, constraint-preserving boundary conditions such as those presented in [11], or higher-order schemes for the hydrodynamic equations such as those presented in [19], would be helpful to further improve the accuracy.

Acknowledgments

It is a pleasure to acknowledge F. Galeazzi, D. Radice and K. Takami for numerous useful discussions. Partial support comes from the DFG grant SFB/Transregio 7, and by “CompStar”, a Research Networking Programme of the European Science Foundation. The calculations were performed on the SuperMUC cluster at the LRZ and on the Datura cluster at the AEI.

-
- [1] R. Arnowitt, S. Deser, and C. W. Misner, in *Gravitation: An introduction to current research*, edited by L. Witten (John Wiley, New York, 1962), pp. 227–265, gr-qc/0405109.
 - [2] J. W. York, in *Sources of gravitational radiation*, edited by L. L. Smarr (Cambridge University Press, Cambridge, UK, 1979), pp. 83–126, ISBN 0-521-22778-X.
 - [3] T. Nakamura, K. Oohara, and Y. Kojima, *Prog. Theor. Phys. Suppl.* **90**, 1 (1987).
 - [4] M. Shibata and T. Nakamura, *Phys. Rev. D* **52**, 5428 (1995).
 - [5] T. W. Baumgarte and S. L. Shapiro, *Phys. Rev. D* **59**, 024007 (1998), gr-qc/9810065.
 - [6] D. Alic, C. Bona-Casas, C. Bona, L. Rezzolla, and C. Palenzuela, *Phys. Rev. D* **85**, 064040 (2012), 1106.2254.
 - [7] S. Bernuzzi and D. Hilditch, *Phys. Rev. D* **81**, 084003 (2010), 0912.2920.
 - [8] M. Ruiz, D. Hilditch, and S. Bernuzzi, *Phys. Rev. D* **83**, 024025 (2011), 1010.0523.
 - [9] A. Weyhausen, S. Bernuzzi, and D. Hilditch, *Phys. Rev.* **D85**, 024038 (2012), 1107.5539.
 - [10] Z. Cao and D. Hilditch, *Phys. Rev. D* **85**, 124032 (2012), 1111.2177.
 - [11] D. Hilditch, S. Bernuzzi, M. Thierfelder, Z. Cao, W. Tichy, and B. Bruegmann, arXiv:1212.2901 (2012), 1212.2901.
 - [12] C. Gundlach, J. M. Martín-García, G. Calabrese, and I. Hinder, *Classical Quantum Gravity* **22**, 3767 (2005), gr-qc/0504114.
 - [13] C. Bona, T. Ledvinka, C. Palenzuela, and M. Zacek, *Phys. Rev. D* **69**, 064036 (2004), gr-qc/0307067.
 - [14] D. Alic, C. Bona, and C. Bona-Casas, *Phys. Rev. D* **79**, 044026

- (2009), 0811.1691.
- [15] B. Giacomazzo and L. Rezzolla, *Classical Quantum Gravity* **24**, S235 (2007), gr-qc/0701109.
- [16] B. Giacomazzo, L. Rezzolla, and L. Baiotti, *Mon. Not. R. Astron. Soc.* **399**, L164 (2009).
- [17] B. Giacomazzo, L. Rezzolla, and L. Baiotti, *Phys. Rev. D* **83**, 044014 (2011).
- [18] F. Galeazzi, W. Kastaun, L. Rezzolla, and J. A. Font, arXiv:1306.4953 (2013), 1306.4953.
- [19] D. Radice, L. Rezzolla, and F. Galeazzi, arXiv:1306.6052 (2013), 1306.6052.
- [20] D. Brown, P. Diener, O. Sarbach, E. Schnetter, and M. Tiglio, *Phys. Rev. D* **79**, 044023 (2009), arXiv:0809.3533 [gr-qc], URL <http://arxiv.org/abs/0809.3533>.
- [21] E. Schnetter, S. H. Hawley, and I. Hawke, *Class. Quantum Grav.* **21**, 1465 (2004).
- [22] P. Colella and P. R. Woodward, *J. Comput. Phys.* **54**, 174 (1984).
- [23] A. Harten, P. D. Lax, and B. van Leer, *SIAM Rev.* **25**, 35 (1983).
- [24] J. Thornburg, *Classical Quantum Gravity* **21**, 743 (2004).
- [25] A. Ashtekar and B. Krishnan, *Living Rev. Relativ.* **7**, 10 (2004), gr-qc/0407042.
- [26] O. Dreyer, B. Krishnan, D. Shoemaker, and E. Schnetter, *Phys. Rev. D* **67**, 024018 (2003), gr-qc/0206008.
- [27] L. Baiotti, B. Giacomazzo, and L. Rezzolla, *Class. Quantum Grav.* **26**, 114005 (2009), 0901.4955.
- [28] W. Tichy, *Phys. Rev. D* **86**, 064024 (2012).
- [29] W. Kastaun, F. Galeazzi, D. Alic, L. Rezzolla, and J. A. Font, arXiv:1301.7348 (2013), 1301.7348.